

Is matter inside massive neutron stars not hadronic?

Presented in XQCD 23, Coimbra

Tuhin Malik

Universidade de Coimbra, Portugal

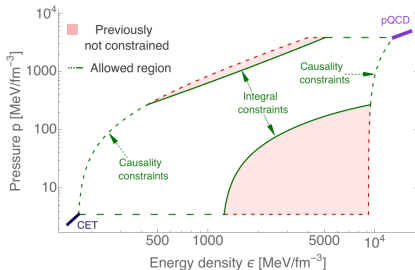


UNIVERSIDADE DE COIMBRA



The dense matter equation of state (EOS)

- ▶ A neutron star (NS), also known as a pulsar, is one of the densest and most compact objects in the universe.
- ▶ A significant probe to reduce uncertainty can be the NS maximum mass, radii, moments of inertia, and tidal Love numbers, which are all accessible to observation.
- ▶ The NS core composition remains a mystery



Phys. Rev. Lett. 128, 202701 (2022), 2111.05350

The possible scenario

- ▶ **nucleon**: Malik et al and B.K. Agrawal et al *Astrophys.J.* 930 (2022), Malik and B.K. Agrawal et al *PRC Letter* 106 (2022), Bikram Keshari Pradhan and Debarati Chatterjee et al *Nucl.Phys.A* 1030 (2023)
- ▶ **hyperons**: S. Weissenborn et al *NPA* 881 (2012), Micaela Oertel et al *EPJA* 52 (2016), Malik and Providência *PRD* 106 (2022)
- ▶ **quark matter**: Annala et al *Nature Phys.*, 16, 907 (2020), Gorda et al *arXiv:2212.10576* (2022)
- ▶ **(anti) kaons**: Banik et al. *Phys.Rev.C* 78 (2008), Char & Banik *Phys. Rev. C* 90(2014), Banik & Bandyopadhyay, *Phys.Rev.C* 64 (2001)
- ▶ **dark matter**
 - ▶ **admixed**: Arpan Das et al *Phys.Rev.D* 99 (2019), Violetta Sagun et al *Phys.Rev.D* 102 (2020)
 - ▶ **two fluid**: Arpan Das et al *Phys.Rev.D* 105 (2022), Violetta Sagun et al *Phys.Rev.D* 105 (2022)
- ▶ **modified gravity**: K. Nobleson et al *JCAP* 08 (2021)

Motivation

- ▶ The agnostic approach:
 - ▶ L. Lindblom et al, Phys. Rev. D 86, 084003 (2012), arXiv:1207.3744.
 - ▶ A. Kurkela et al, Astrophys. J. 789, 127 (2014), arXiv:1402.6618.
 - ▶ E. R. Most et al, Phys. Rev. Lett. 120, 261103 (2018), arXiv:1803.00549.
 - ▶ E. Lope Oter et al, J. Phys. G 46, 084001 (2019), arXiv:1901.05271.
 - ▶ E. Annala et al, Nature Phys. 16, 907 (2020), arXiv:1903.09121., E. Annala et al, arXiv:2105.05132
 - ▶ Rahul Somasundaram et al, arXiv : 2112.08157
 - ▶ Sinan Altiparmak et al, arXiv: 2203.14974
- ▶ What do a minimal set of nuclear matter constraints together with a $2M_{\odot}$ condition tell us about the NS EOS based on a microscopic model?
- ▶ Can we extract nuclear matter properties from neutron star matter EOS?

Relativistic description of the neutron star equation of state (a Bayesian approach)

EOS: relativistic mean field description

RMF Lagrangian for stellar matter

▶ Lagrangian density

- ▶ Lorentz-covariant Lagrangian with baryon densities and meson fields
- ▶ causal by construction

$$\mathcal{L} = \mathcal{L}_N + \mathcal{L}_M + \mathcal{L}_{NL},$$

▶ Baryonic contribution:

$$\mathcal{L}_N = \bar{\Psi} \left[\gamma^\mu \left(i\partial_\mu - \Gamma_\omega \mathbf{A}_\mu^{(\omega)} - \Gamma_\rho \mathbf{t} \cdot \mathbf{A}_\mu^{(\rho)} \right) - (m - \Gamma_\sigma \phi) \right] \Psi,$$

▶ Meson contribution

$$\begin{aligned} \mathcal{L}_M = & \frac{1}{2} \left[\partial_\mu \phi \partial^\mu \phi - m_\sigma^2 \phi^2 \right] - \frac{1}{4} F_{\mu\nu}^{(\omega)} F^{(\omega)\mu\nu} + \frac{1}{2} m_\omega^2 \omega_\mu \omega^\mu \\ & - \frac{1}{4} \mathbf{F}_{\mu\nu}^{(\rho)} \cdot \mathbf{F}^{(\rho)\mu\nu} + \frac{1}{2} m_\rho^2 \boldsymbol{\rho}_\mu \cdot \boldsymbol{\rho}^\mu. \end{aligned}$$

- ▶ (i) density dependent couplings are introduced (DDH and DDB models); (ii) non-linear mesonic terms are included (NL)

Density dependent description

The density dependent models include meson-nucleon couplings Γ_i , that depend on the total nucleonic density ρ , and is defined as

$$\Gamma_i(\rho) = \Gamma_{i,0} h_i(x) , \quad x = \rho/\rho_0 , \quad i = \sigma, \omega, \rho, \quad (1)$$

with $\Gamma_{i,0}$ the couplings at saturation density ρ_0 . For the isoscalar mesons, σ and ω , two parametrizations h_i are considered:

$$h_i(x) = \exp[-(x^{a_i} - 1)] \quad (2)$$

as in Malik et al. 2022, giving origin to the DDB sets, and

$$h_i(x) = a_M \frac{1 + b_i(x + d_i)^2}{1 + c_i(x + d_i)^2} , \quad (3)$$

as in Typel and Wolter 1999; Typel, Ropke, et al. 2010, and originating the DDH data sets. The ρ -meson nucleon coupling is defined as in Typel and Wolter 1999

$$h_\rho(x) = \exp[-a_\rho(x - 1)] . \quad (4)$$

Non-linear meson terms

The model introduced in Mueller and Serot 1996 is defined with constant couplings, which we designate by g_i , $i = \sigma, \omega, \rho$, and, instead, includes non-linear meson terms in the Lagrangian density, which are defined by

$$\mathcal{L}_{NL} = -\frac{1}{3}bg_{\sigma}^3(\sigma)^3 - \frac{1}{4}cg_{\sigma}^4(\sigma)^4 + \frac{\xi}{4!}(g_{\omega}\omega_{\mu}\omega^{\mu})^4 \\ + \Lambda_{\omega}g_{\rho}^2\boldsymbol{\rho}_{\mu} \cdot \boldsymbol{\rho}^{\mu}g_{\omega}^2\omega_{\mu}\omega^{\mu}$$

The parameters multiplying each one of these terms b , c , ξ , Λ_{ω} will be fixed together with the meson-nucleon couplings g_i by imposing nuclear matter and NS observational constraints. The parameters b , c , in front of the σ self interacting terms control the nuclear matter incompressibility at saturation Boguta and Bodmer 1977. The ξ term was introduced in Sugahara and Toki 1994 to modulate the high density dependence of the EoS, the larger ξ the softer the EOS. The non-linear $\omega - \rho$ term influences the density dependence of the symmetry energy Cavagnoli, Menezes, and Providencia 2011.

Nuclear matter properties at saturation

- Taylor expansion, parabolic approximation

$$\frac{E_{\text{nuc}}}{A}(n, \delta) = \frac{E_{\text{SNM}}}{A}(n) + S(n) \delta^2,$$

$$S(n) = \frac{1}{2} \left. \frac{\partial^2 E_{\text{nuc}}/A}{\partial \delta^2} \right|_{\delta=0},$$

$$\frac{E_{\text{SNM}}}{A}(n) = E_0 + \frac{K_0}{2} \eta^2 + \frac{J_0}{3!} \eta^3 + \frac{Z_0}{4!} \eta^4,$$

$$S(n) = E_{\text{sym}} + L_{\text{sym}} \eta + \frac{K_{\text{sym}}}{2} \eta^2 + \frac{J_{\text{sym}}}{3!} \eta^3 + \frac{Z_{\text{sym}}}{4!} \eta^4,$$

$$\delta = (n_p - n_n)/n, \quad \eta = (n - n_0)/(3n_0)$$

Bayesian estimation of model parameters

Bayesian Inference:

$$P(\theta | D) = \frac{\mathcal{L}(D | \theta)P(\theta)}{\mathcal{Z}}$$

- ▶ The θ is the model parameter vector and D is the set of fit data.
- ▶ $P(\theta | D)$ is the joint posterior distribution of the parameters.
- ▶ $\mathcal{L}(D | \theta)$ is the likelihood function.
- ▶ $P(\theta)$ is the prior distribution for the model parameters.
- ▶ \mathcal{Z} is the evidence. It can be obtained by complete marginalization of the likelihood function.

The marginalized posterior distribution for a parameter θ_i :

$$P(\theta_i | D) = \int P(\theta | D) \prod_{k \neq i} d\theta_k$$

Gaussian likelihood function

$$\mathcal{L}(D | \theta) = \prod_j \frac{1}{\sqrt{2\pi\sigma_j^2}} e^{-\frac{1}{2} \left(\frac{d_j - m_j(\theta)}{\sigma_j} \right)^2}$$

- ▶ The index j runs over all the data points.
- ▶ The d_j and m_j are the data and corresponding model values, respectively.
- ▶ The σ_j are the uncertainties for every data point.

The fit data

| Constraints | | | |
|--------------------------------|--------------------|--------------------------------|---|
| Quantity | | Value/Band | Ref |
| NMP (MeV) | ρ_0 | 0.153 ± 0.005 | Typel & Wolter (1999) |
| | ϵ_0 | -16.1 ± 0.2 | Dutra et al. (2014) |
| | K_0 | 230 ± 40 | Todd-Rutel & Piekarewicz (2005); Shlomo et al. (2006) |
| PNM (MeV fm^{-3}) | $J_{\text{sym},0}$ | 32.5 ± 1.8 | Essick et al. (2021a) |
| | $P(\rho)$ | $2 \times \text{N}^3\text{LO}$ | Hebeler et al. (2013) |
| NS mass (M_\odot) | M_{max} | >2.0 | Fonseca et al. (2021) |

NL, DDB and DDH: a comparison

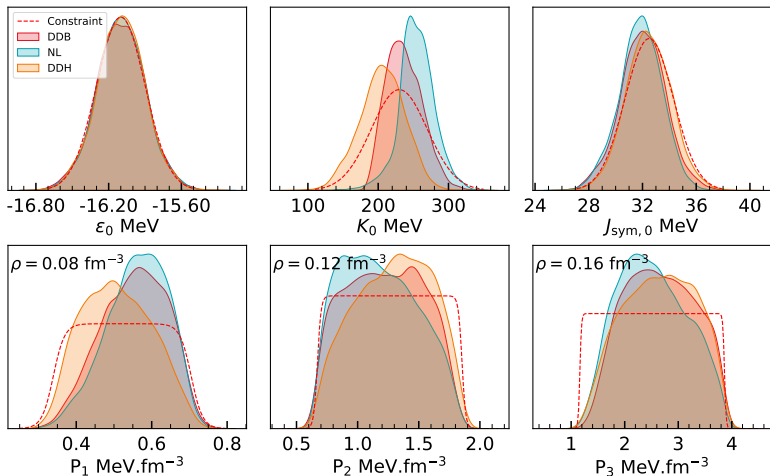
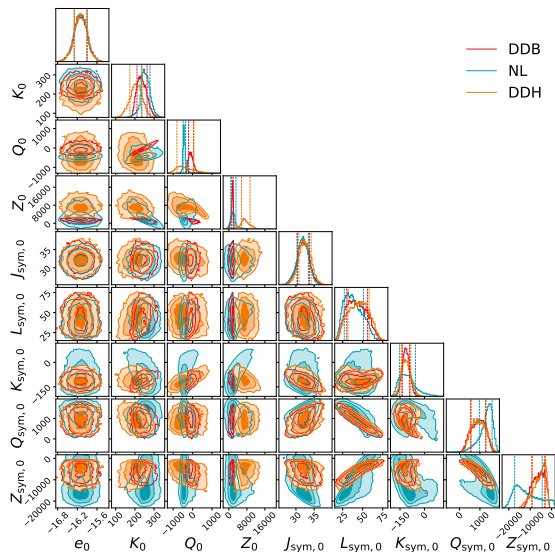


Figure: Fit data considered to constrain all EOS data set built for the present study, both for nucleonic and for hyperonic matter.

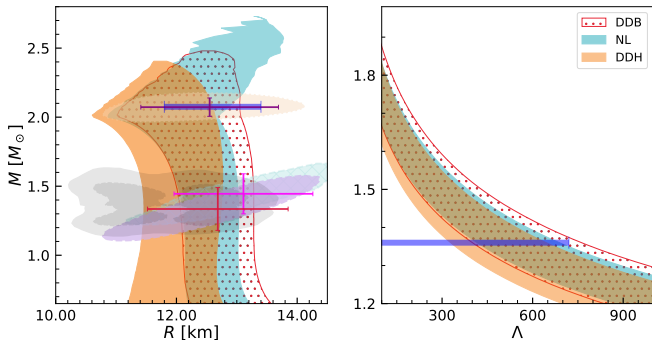
Nuclear matter properties

Posterior



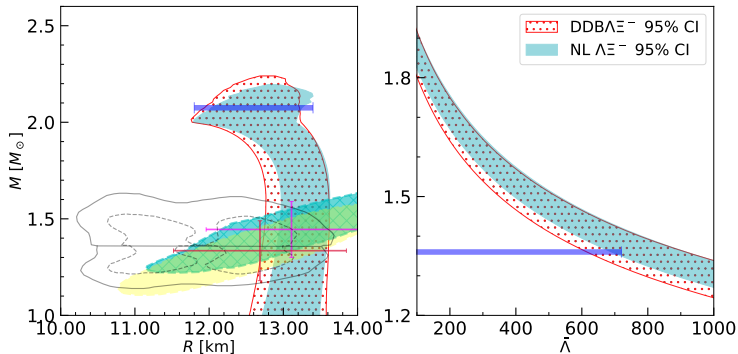
- ▶ The incompressibility of DDH models peaks at lower values compared to the other two models. It also spreads over a larger range of values.
- ▶ DDH exhibits a wide spread of skewness values, ranging from low negative to high positive values. The kurtosis in DDH takes the largest values to compensate for the low incompressibility values, satisfying the $2M_{\odot}$ constraint.
- ▶ The symmetry energy and slope at saturation are similar for all three models, but there are differences in higher order parameters such as $K_{\text{sym},0}$ and $Z_{\text{sym},0}$. DDH and DDB behave similarly, while NL exhibits a wider range of values for these parameters.

The neutron star properties



The blue horizontal bar on the left panel indicates the 90% CI radius for the pulsar PSR J0740+6620 with $M = 2.08M_{\odot}$ obtained combining observational data from GW170817 and NICER as well as nuclear saturation properties Miller et al. 2021. The gray shaded regions indicate the 90% (solid) and 50% (dashed) CI of the LIGO/Virgo analysis for high mass (top) and low mass (bottom) components of the NS binary that originated the GW170817 event Abbott et al. 2019. The NICER 1σ (68%) credible zone of the 2-D mass-radii posterior distribution for the PSR J0030+0451 (lilas and light green) Riley et al. 2019; Miller et al. 2019, and the PSR J0740 + 6620 (light orange) Riley et al. 2021; Miller et al. 2021 are also included. The horizontal (radius) and vertical (mass) error bars reflect the 1σ credible interval derived for NICER data's 1-D marginalized posterior distribution.

Including hyperons

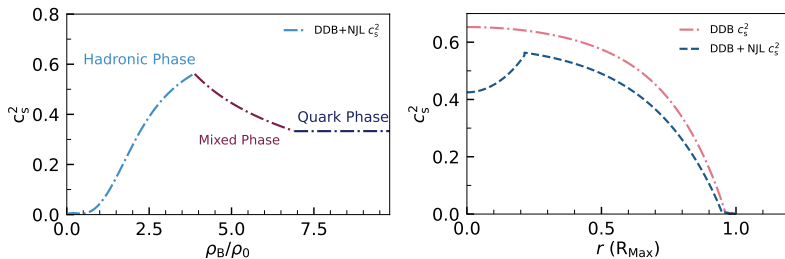


The 90% CI region for the hyperon data sets DDB-hyp (dotted red) and NL-hyp (green) derived using the conditional probabilities $P(R|M)$ (left) and $P(\tilde{\lambda}|M)$ (right). The lines in the left panel indicate the 90% (solid) and 50% (dashed) CI for the binary components of the GW170817 event Abbott et al. 2019. Also shown is the 1σ (68%) credible 2-D posterior distribution in the mass-radii domain from the millisecond pulsar PSR J0030+0451 Riley et al. 2019; Miller et al. 2019 obtained from the NICER x-ray data. The horizontal (radius) and vertical (mass) error red bars reflect the 1σ credible interval derived for the same NICER data's 1-D marginalized posterior distribution. The blue bars represent the radius of the PSR J0740+6620 at $2.08M_{\odot}$ (left panel) and the tidal deformability at $1.36M_{\odot}$ (right panel) Abbott et al. 2018.

Comments

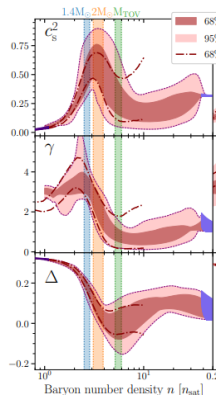
- ▶ The median values of the radius of $1.4 M_{\odot}$ stars reflect clearly this effect: they increase from 12.66 (12.44) km for DDB (NL) to 14.22 (13.11) km, i.e. more than ~ 0.5 km or $\sim 5\%$.
- ▶ Measurements of the NS radius with an uncertainty smaller than 5%, such as the ones programmed with eXTP Watts 2019 and STROBE-X Ray 2019, could distinguish between these two scenarios.
- ▶ The tidal deformability is strongly affected increasing its median value from 466 (423) to 650 (610), respectively, for DDB (NL), and the constraint imposed by GW170817 is essentially not satisfied.
- ▶ Another important property that distinguishes both scenarios is the NS maximum mass that decreases from a maximum value at 90% CI of 2.37 (2.26) M_{\odot} for DDB (NL) to 2.08 (2.13) M_{\odot} .

Speed of sound in hybrid stars



Deepak Kumar, Hiranmaya Mishra, Tuhin Malik, JCAP 02 (2023) 015

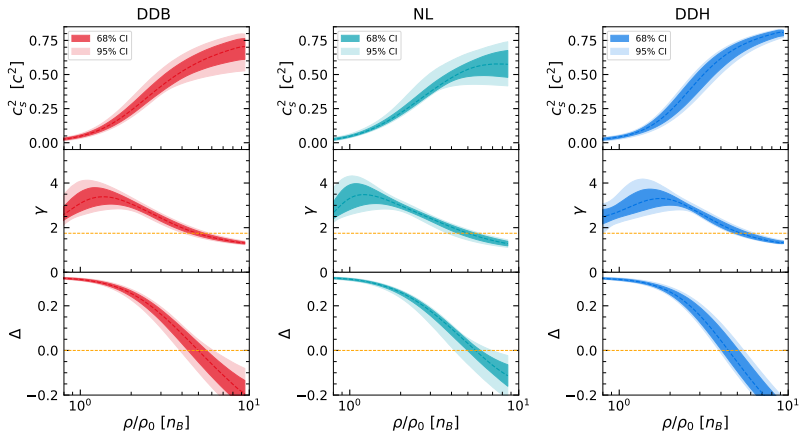
Speed of sound, trace anomaly, and pQCD constraints



- ▶ polytropic index $\gamma = d \ln P / d \ln \epsilon$ Annala, Gorda, Kurkela, et al. 2020, which takes the value 1 in conformal matter, the trace anomaly scaled by the energy density introduced in Fujimoto et al. 2022 $\Delta = 1/3 - P/\epsilon$ which should approach zero in the conformal limit, and the derived quantity proposed in Annala, Gorda, Hirvonen, et al. 2023

$$d_c = \sqrt{\Delta^2 + \Delta'^2}, \text{ where } \Delta' = c_s^2 (1/\gamma - 1) \text{ is the logarithmic derivative of } \Delta \text{ with respect to the energy density, which approaches zero in the conformal limit.}$$

- ▶ The general behavior of the speed of sound squared obtained from agnostic descriptions of the EOS of baryonic matter, that has been constrained by low-density pure neutron matter *ab-initio* calculations Hebeler et al. 2013; Drischler, Hebeler, and Schwenk 2019; Drischler, Melendez, et al. 2020 and the pQCD EOS at densities of the order $\gtrsim 40\rho_0$, and by NS observations, includes a steep increase until an energy density of the order of ~ 500 MeV/fm is attained, followed by a decrease or flattening, approaching 1/3 at high densities Annala, Gorda, Kurkela, et al. 2020; Altiparmak, Ecker, and Rezzolla 2022; Somasundaram, Tews, and Margueron 2023; Gorda, Komoltsev, and Kurkela 2022; Kurkela 2022; Annala, Gorda, Hirvonen, et al. 2023, see also the discussion in Kojo 2021.



The speed of sound squared c_s^2 , the polytropic index $\gamma = d \ln P / d \ln \epsilon$ and the trace anomaly $\Delta = 1/3 - P/\epsilon$ for the three data sets, DDB, NL and DDH. The horizontal lines in the γ plots identifies the value 1.75.

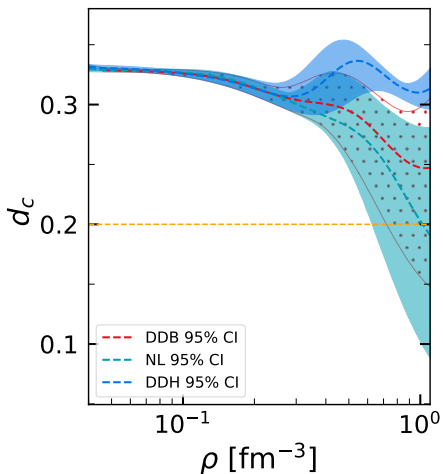
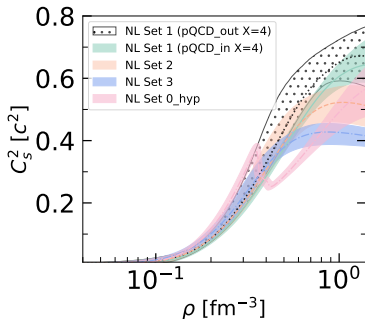
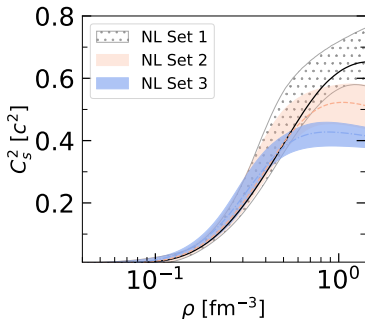


Figure: The figure illustrates the relationship between d_c and ρ for three data sets: DDB, NL, and DDH, arranged from left to right. The median values are represented by lines, while the 95% confidence interval regions are depicted as shaded bands.



The figure displays the median and 95% credible interval of the square of sound velocity (c_s^2) for the NL model. The left panel highlights three distinct intervals of the parameter ξ : NL Set 1, NL Set 2, and NL Set 3. In the plot, NL Set 1 is represented by a black dotted region and corresponds to ξ values within the interval [0, 0.004]. NL Set 2 is represented by an orange region and encompasses ξ values within the range [0.004, 0.015]. NL Set 3 is depicted in blue and represents ξ values within the interval [0.015, 0.04]. Each set of EOS contains a comparable number of samples, approximately 18,000 samples, providing a robust statistical basis for the displayed results. In the right panel, Set 1 was divided into two parts: green (black dotted) EoS that satisfy (do not satisfy) pQCD constraints with $X=4$. In this panel the c_s^2 for the NL-hyp set is also shown (pink band).

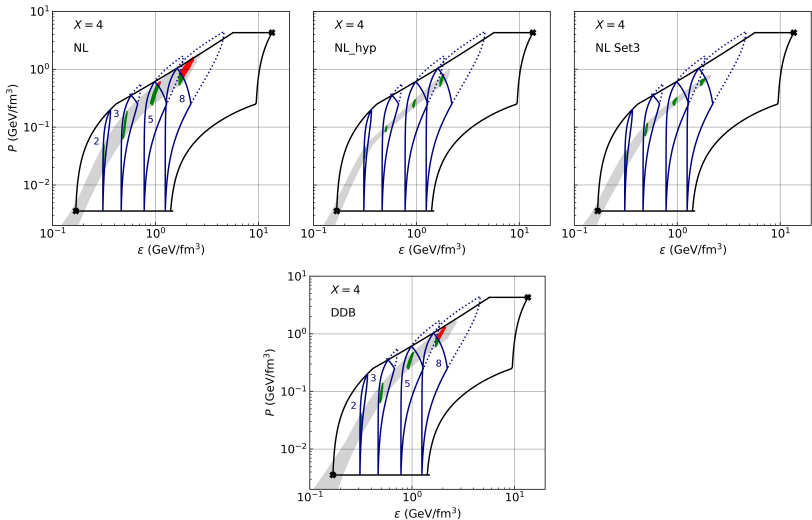


Figure: The pressure versus the energy density is shown for NL, NL-hyp and NL restricted to $\xi \in [0.015 : 0.04]$ (set 3) (top line, from left to right) and DDB (bottom line). The constraints from Ref. Komoltsev and Kurkela 2022 that ensure stability, causality, and thermodynamic consistency delimit the region inside the black solid line.

Conclusions

- ▶ Bayesian inference was used to determine the probability distribution of coupling parameters and calculate nuclear matter properties (NMP) and neutron star (NS) properties. The posterior distributions of the three data sets (fit-data, pure neutron matter pressure, and maximum star mass) showed non-coincidence in the mass-radius domain at 90% confidence intervals.
- ▶ The inclusion of hyperons in the models does not exclude the existence of $2M_{\odot}$ stars, although the maximum masses obtained with hyperonic models are smaller than nucleonic models. However, introducing hyperonic degrees of freedom leads to larger radii for canonical stars due to the softening of the equation of state (EOS) and the requirement for larger nuclear matter parameters.
- ▶ The speed of sound behavior within DDH and DDB models is monotonically increasing with density, while the NL model's behavior is sensitive to the coupling of the ω^4 term. The NL model may exhibit a maximum speed of sound followed by a decreasing tendency with density, resembling a non-nucleonic degree of freedom onset. The lack of constraining high-density observations or experimental data contributes to the different behaviors of the three frameworks.
- ▶ The three models predict polytropic indices below 1.75 for densities above 0.4 to 0.7 fm^{-3} , and the trace anomaly becomes negative for these densities. The quantity related to the trace anomaly, d_c , proposed in a study, generally takes values above 0.2, considered a transition to deconfined quark matter. However, the NL and DDB models do not exclude values below 0.2 at densities above $\gtrsim 0.6 \text{ fm}^{-3}$, although all three models have d_c values below 0.35.
- ▶ By considering thermodynamic, causality, low-density nuclear matter, and high-density pQCD constraints, models within RMF that do not satisfy high-density constraints were identified. These models exhibit a very stiff high-density EOS but remain causal.

ACKNOWLEDGMENTS

The authors acknowledge the Laboratory for Advanced Computing at the University of Coimbra for providing HPC resources (Navigator+) that have contributed to this research results.

Data availability

- ▶ [10.5281/zenodo.7854112](https://zenodo.org/record/7854112)
- ▶ [10.5281/zenodo.6342100](https://zenodo.org/record/6342100)

Article

- ▶ Neutron star equation of state: identifying hadronic matter characteristics, Constança Providência, Tuhin Malik, Milena Bastos Albino, Márcio Ferreira, e-Print: 2307.05086
- ▶ Phys.Rev.D 107 (2023) 10, 103018, Phys.Rev.D 106 (2022) 6, 063024, Astrophys.J. 930 (2022) 1, 17.

ACKNOWLEDGMENTS

- ▶ Constança Providência, Helena Pais, Márcio Ferreira, Milena Bastos Albino
- ▶ Veronica Dexheimer
- ▶ Hiranmaya Mishra, Deepak Kumar
- ▶ B.K. Agrawal, Sk Md. Adil Imam, N.K. Patra
- ▶ Débora P. Menezes, Kauan D. Marquez

Thank you!

Obrigado!

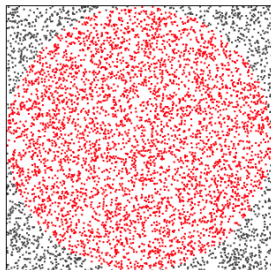
THE BAYESIAN SETUP

By updating a prior belief (i.e., a prior distribution) with given information (i.e., observed or fit data) and optimizing a likelihood function, a posterior distribution can be obtained according to Bayes' theorem.

- ▶ The prior
- ▶ The fit data
- ▶ The Log-Likelihood
- ▶ The sampling algorithm

Sampling

Monte Carlo sampling:



- ▶ Generate random uniform samples in the parameter hyperspace.
- ▶ Apply filter
- ▶ Analyze filtered samples' properties

Markov Chain Monte Carlo sampling:

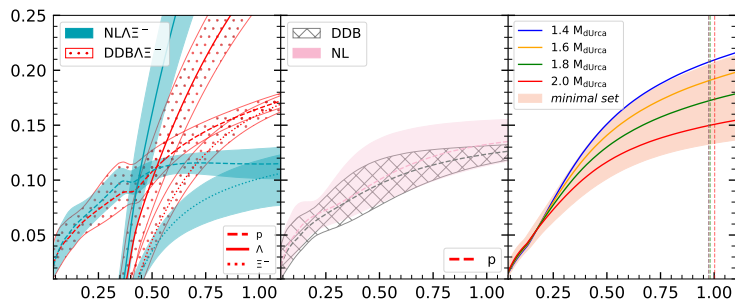
- ▶ Cost-function guided random walk
- ▶ Sample the posterior

we use the nested sampling algorithm, first proposed in J Skilling, American Institute of Physics Conference Series, Vol. 735, edited by R. Fischer, R. Preuss, and U. V. Toussaint (2004) pp. 395–405.

- ▶ suitable for low-dimensional problems
- ▶ approximately 17000 samples we have obtained in the posterior

Onset of direct Urca

The dependence on the baryon density of the proton fraction of β -equilibrium matter will be discussed.



Proton and hyperons fractions for data sets DDB-hyp (red dotted) and NL-hyp (blue) (left panel), proton fractions for the data sets DDB (slashed region) and NL (pink region) (middle panel), proton fraction defining the minimal set compatible with chEFT PNM calculations at 2σ obtained varying the parameter y introduced in Eq. (5) (pink region), or fixing y to a given M_{dUrca} , i.e. 1.4, 1.6, 1.8, 2.0 M_\odot (full lines).

$$h_\rho(x) = y \exp[-a_\rho(x - 1)] + (y - 1), \quad 0 < y \leq 1. \quad (5)$$

Comments

- ▶ The ρ -meson coupling: in DDB and DDH data sets decreases exponentially with density, approaching zero at high densities. This leads to very asymmetric matter at high densities due to the low symmetry energy, preventing the occurrence of nucleon direct Urca processes inside neutron stars (NS).
- ▶ The proton fraction in DDB data set is smaller and narrower than in the NL data set at large densities, indicating that the g_ρ coupling tends to zero for all models at high densities. NL models have a wider range of proton fractions, and direct Urca processes may occur in some models.
- ▶ The Λ hyperon appears just above twice saturation density, reducing the neutron fraction and consequently decreasing the system energy. The Ξ^- hyperon sets in just below $3 \rho_0$, causing an increase in the proton fraction to compensate for the negatively charged hyperon.
- ▶ Introducing a new parameter γ that affects the high-density behavior of the symmetry energy. The determination of γ is based on NS properties sensitive to the symmetry energy, such as the onset of nucleon direct Urca processes.

NMP

| Model | ρ_0 fm^{-3} | ϵ_0 | K_0 | Q_0 | Z_0 | $J_{\text{sym},0}$ | $L_{\text{sym},0}$ | $K_{\text{sym},0}$ | $Q_{\text{sym},0}$ | $Z_{\text{sym},0}$ | | |
|-------|------------------------------|--------------|--------|--------|-------|--------------------|--------------------|--------------------|--------------------|--------------------|--------|--------|
| | MeV | | | | | | | | | | | |
| DDB | median | 0.152 | -16.10 | 235 | -90 | 1585 | 32.05 | 42 | -114 | 935 | -5941 | |
| | 90 % CI | min | 0.142 | -16.43 | 199 | -262 | 486 | 29.15 | 25 | -149 | 364 | -10751 |
| | | max | 0.164 | -15.76 | 282 | 162 | 2043 | 34.81 | 63 | -76 | 1434 | -2128 |
| NL | median | 0.152 | -16.10 | 254 | -440 | 1952 | 31.89 | 37 | -109 | 1367 | -12613 | |
| | 90 % CI | min | 0.145 | -16.43 | 213 | -516 | 243 | 29.08 | 23 | -171 | 629 | -19118 |
| | | max | 0.160 | -15.77 | 297 | -247 | 5295 | 34.41 | 58 | -3 | 1710 | -394 |
| DDH | median | 0.156 | -16.10 | 206 | -460 | 7189 | 32.44 | 45 | -114 | 930 | -5215 | |
| | 90 % CI | min | 0.144 | -16.43 | 150 | -978 | 4459 | 29.68 | 25 | -157 | 412 | -11529 |
| | | max | 0.167 | -15.78 | 257 | 395 | 10908 | 35.24 | 65 | -64 | 1491 | -2078 |

The Log-Likelihood

The equation 6 shows the log-likelihood function, except for the low-density PNM data and the maximum mass of NS. Our approach has been to use the box function probability as given in equation 7 for the PNM data from χ EFT. We also used the step function probability for the NS mass.

$$\text{Log}(\mathcal{L}) = -0.5 \times \sum_j \left\{ \left(\frac{d_j - m_j(\theta)}{\sigma_j} \right)^2 + \text{Log}(2\pi\sigma_j^2) \right\} \quad (6)$$

$$\text{Log}(\mathcal{L}) = \text{Log} \left\{ \prod_j \frac{1}{2\sigma_j} \frac{1}{\exp\left(\frac{|d_j - m_j(\theta)| - \sigma_j}{0.015}\right) + 1} \right\} \quad (7)$$

*

*It is important to understand that when sampling the posterior, the normalization of the log-likelihood, which is done in equations 6 and 7 is irrelevant. However, to calculate the Bayes *evidence* it is mandatory and in some cases, it also reduces the computation time.